Flow Structures of the Benthic Ocean

LAURENCE ARMI AND ERIC D'ASARO

Woods Hole Oceanographic Institution, Woods Hole, Massachusetts 02543

Three-dimensional structure of the near-bottom density field was observed with a towed yo-yoing profiler and a fixed current/temperature measuring array on the Hatteras abyssal plain. A great variety of structures were seen. Immediately above the bottom a well-mixed bottom layer extends vertically 5–60 m, with less than 1 m°C potential temperature change. This mixed layer is often capped by a region of strong vertical potential temperature gradient, with up to 100-m°C potential temperature change in ~10 m. The boundary layer may be uniform for 10 km or exhibit a bottom temperature gradient of up to 20 m°C/km. Interior layers of nearly constant potential temperature and horizontal extent of 2–100 km are seen ~25% of the time above the bottom mixed layer. When an interior layer is present, the bottom mixed layer is thinner. On many occasions an interior layer was seen to be horizontally continuous with the bottom mixed layer, suggesting formation of interior layers by detachment of the bottom mixed layer. A benthic front was observed. Differential horizontal advection is required to explain the observed structures. Velocity fluctuations above 1 cph increase in energy near the bottom, presumably a signature of turbulence in the mixed layer; these fluctuations are modulated by the passage of structures observed in the moored record.

1. Introduction

The benthic boundary layer is a region adjacent to the ocean bottom with characteristics distinct from the oceanic interior. Near the bottom it is turbulent, and the resultant mixing is seen as a bottom layer homogeneous in salinity and potential temperature [*Armi and Millard,* 1976; *Eittreim et al.,* 1975; *Greenewalt and Gordon,* 1978; *Pak and Zaneveld,* 1977; *Weatherly and Niiler,* 1974; *Wimbush and Munk,* 1970]. This layer is the benthic analog of the atmospheric boundary layer and may be similar to the oceanic surface mixed layer. This paper reports on the three-dimensional structure of the near-bottom density field as observed with a towed yo-yoing profiler and a fixed current/temperature measuring array.

In a previous study, *Armi and Millard* [1976] described boundary layer density profiles taken in the western North Atlantic as part of the Mid-Ocean Dynamics Experiment (Mode). They found that simple mixed layers generally occurred over the Hatteras abyssal plain, while irregular structures, commonly with multiple layers, occurred near rough topography. In a short time series at the edge of the plain they observed a doubling of the mixed layer height in less than a day. The Hatteras abyssal plain was chosen for the location of the intensive benthic boundary layer experiment described here both because of the previously observed simple structures and because the interior flow in this area has been extensively studied [cf. *Mode Group,* 1978; *Briscoe,* 1975].

Sections 2 and 3 describe the experiment and the data calibration and display. A detailed discussion of the observations follows in section 4, which is summarized in section 5. Section 6 discusses these results.

2. Description of the Experiment

This experiment was designed to measure the density and velocity structure in both space and time near the ocean bottom. A 3-month time series, May 18, 1977, to August 18, 1977, of velocity and temperature was measured by two bottom morrings (Figure 1) deployed near 28°30′N, 70°30′W by the Moored Array Project of the Woods Hole Oceanographic Institution (WHOI). The Hatteras abyssal plain is extremely flat with a slope of only 20 cm/km over hundreds of kilometers [*Bush,* 1976]. Mooring A (WHOI 621) contained vector-averaging current meters spaced so as to span the mixed layers seen by *Armi and Millard* [1976]. Note that instruments 1 and 2 are separated by 20 m, while the other instruments are separated by 10 m. Each instrument recorded vector average velocity and average temperature every 7½ min. In addition, the bottom six instruments measured the average differential temperature between the top and the bottom of the instrument case (1.74 m), as described by *Dean* [1979]. Mooring B (WHOI 622), 4.3 km to the east, contained a single vector-averaging current meter measuring average velocity and temperature every 7½ min.

Three spatial surveys of the boundary layer were made: The first was made on cruise *Knorr* 66 and the second two on cruise *Oceanus* 31. Station positions are shown in Figure 2. Moorings A and B and a third bottom-moored beacon, C, formed an acoustic navigation net [*Phillips et al.,* 1979]. By using acoustic navigation the ship and an instrument package could be located to within 10 m with respect to the moorings. Loran C was also used and provided navigational data outside the acoustic range.

A photograph of the instrument package and a preliminary description of these experimental results can be found in the paper by *Armi* [1978*b*]. A Neil Brown conductivity, temperature, and depth profiler (CTD); a nephelometer built at the Woods Hole Oceanographic Institution; a General Oceanics rosette water sampler; an acoustic transponder (AMF acoustic release); and a Benthos pinger were enclosed in a protective frame which was lowered from the ship. The bottom pinger and a precision depth recorder were used to bring the instruments to within 2 m of the bottom. Actual bottom pressure was determined by occasionally setting the instrument package gently on the bottom. The bottom pressure was always 5555 dbar. The CTD and nephelometer data were available in real time on the ship. On some stations a string of Niskin bottles and a Thorndike nephelometer [*Thorndike,* 1975] were attached to the wire. The Niskin bottom water samples were analyzed for radon 222 and particulate matter concentrate. Results of the Thorndike nephelometer, particulate mat-

Paper number 9C1353.
0148-0227/80/009C-1353$01.00

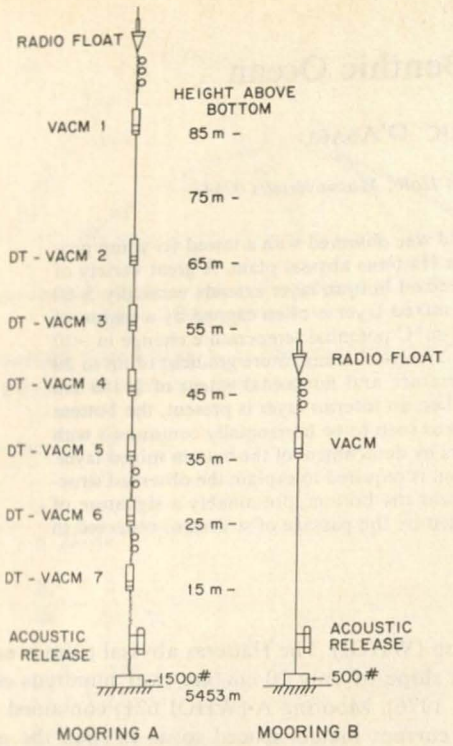

Fig. 1. Mooring diagram for the benthic boundary layer experiment. All vector-averaging current meters (VACM) measure vector mean current and temperature. Differential temperature VACM's (DT-VACM) also measure temperature differences between the top and the bottom of the 1.74-m instrument case. The acoustic releases contain transponders and in conjunction with a third transponder, beacon C (not shown), formed an acoustic navigation net.

ter concentration, and radon measurements will be reported elsewhere by P. E. Biscaye and J. L. Sarmiento.

3. Data Calibration, Processing, and Display

Conductivity, temperature, depth profiler. This instrument was calibrated as described by *Fofonoff et al.* [1974]. CTD data were edited by rejecting up to 0.33 s worth of data if the forward first difference of pressure or temperature was large. At a typical near-bottom lowering speed of 30 m/min, only spikes associated with a vertical scale smaller than 16 cm were rejected. Only CTD downtraces were used. Uptraces were found to be consistently colder and to contain numerous temperature inversions presumably caused by the wake of the instrument package. A few downtraces were similarly contaminated, principally in towed stations. Different CTD instruments were used on each of the two cruises, *Knorr* 66 and *Oceanus* 31.

Historically, the deepwater potential temperature/salinity relation in this region is exact within measurement error [*Worthington and Metcalf*, 1961; *Mode-1 Atlas Group*, 1977]. No deviation from a constant relationship was found in the CTD data. If salinity is considered a function of potential temperature, it can be predicted about 10 times more accurately than it can be measured by the CTD. Therefore potential temperature alone can measure density at least as accurately as can potential temperature and salinity. Thus only potential temperature relative to the ocean surface, computed as described by *Fofonoff* [1977], will be displayed. By using the *Worthington and Metcalf* [1961] potential temperature/salinity relationship, potential density changes referenced to 5500 dbars are related to potential temperature changes by $g(\Delta\rho/\rho) = -0.10\Delta\theta$.

Vector-averaging current meters (VACM). The instruments used in this experiment have a Savonius rotor and a vane to measure the horizontal current [*McCullough*, 1975]. The rotors from VACM's 2–7 on mooring A were individually calibrated after the experiment in a flume at the Woods Hole Oceanogrpahic Institution. A mean stall speed of 1.3 cm/s was found (J. Dean, personal communication, 1979). The estimated speed calibration error is ±0.2 cm/s. In data processing, rotor stalls were assigned a speed of zero rather than the usual 2.0 cm/s. *Bryden* [1976] estimates an rms instrumental direction bias of about 2° for the VACM.

The measured VACM temperature variations have a precision of better than a millidegree (±1 m°C). The absolute tem-

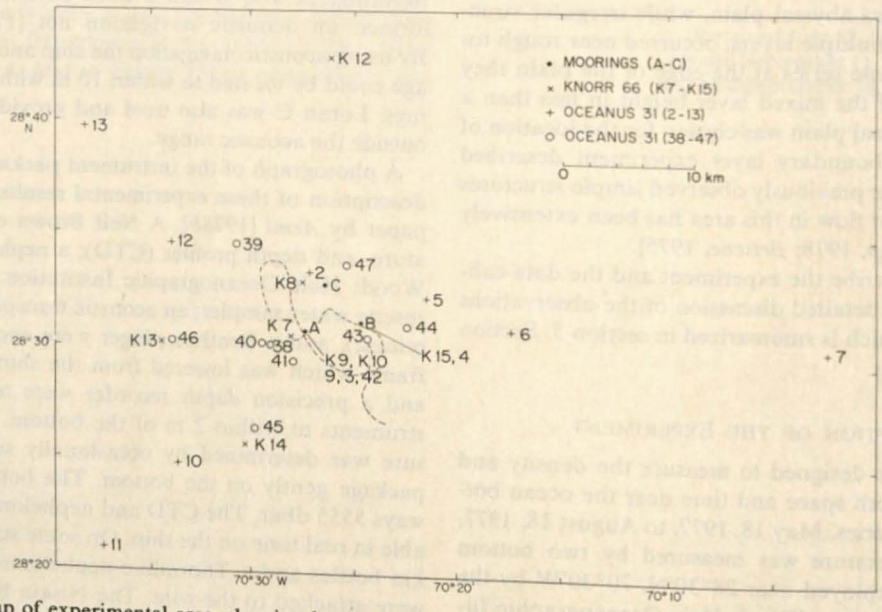

Fig. 2. Map of experimental area, showing locations of moorings and CTD profiler stations. Dashed lines show the track of *Oceanus* 31 towed stations 38 and 43. A larger-scale map is shown in Figure 13. Times for CTD stations are marked in Plate 1.

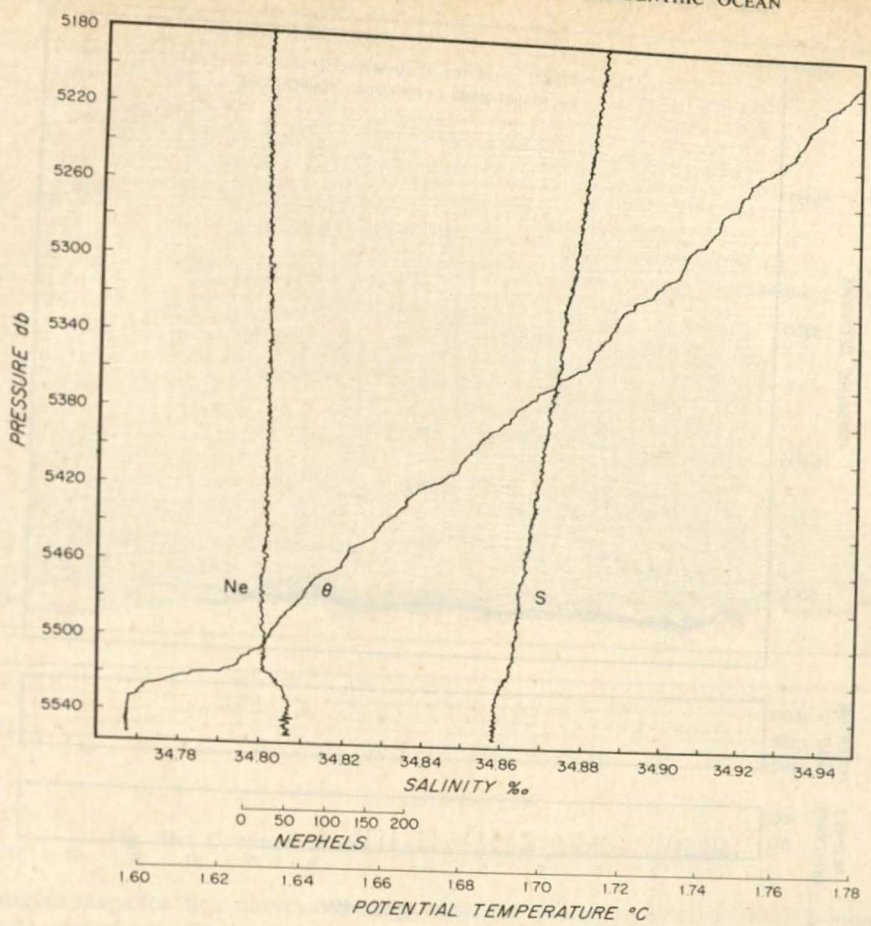

Fig. 3. Profiles of potential temperature, salinity, and nephels (turbidity) from the first downtrace of *Oceanus* 31, station 38.

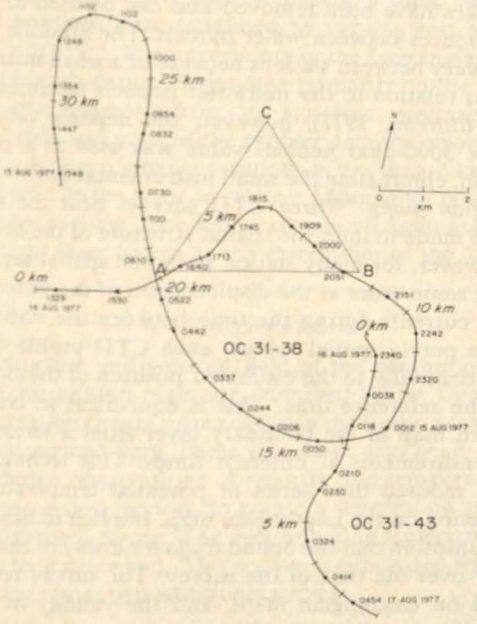

Fig. 4. Paths of *Oceanus* 31 towed CTD yo-yo stations 38 and 43, as determined by acoustic navigation, annotated with time and distance along track. The positions of moorings A and B and beacon C are shown.

perature calibrations, however, have an accuracy of about 5–10 m°C [*Payne et al.*, 1976]. The VACM temperatures have been calibrated in situ as follows: CTD measurements of the bottom mixed layer reveal it to be almost always homogeneous in potential temperature to within 1 m°C. Whenever a given instrument showed a constant differential temperature, it was assumed to be in a mixed layer. Whenever two adjacent instruments were in a mixed layer, they were assumed to be measuring the same potential temperature. Over a period of 3–4 years, VACM 5 has had a low-temperature calibration drift of 1 m°C/yr (R. E. Payne, personal communication, 1979). The temperature measured by VACM 5 was used as a reference. For example, on July 30, instruments 5–7 were in a mixed layer; thus the temperatures of VACM's 7 and 6 were shifted until they agreed with VACM 5. In addition, instrument pairs that showed temperature inversions greater than 0.5 m°C for longer than 40 min were shifted to remove the inversion. There were sufficient mixed layers, some detached from the bottom, to provide a consistent potential temperature calibration for all the VACM's on mooring A. For the deeper instruments, enough mixed layers were present to determine both an offset and a drift. The rms magnitude of the offsets relative to instrument 5 was 11 m°C. The maximum drift was 7 m°C over the 3-month duration of the experiment.

Several CTD stations were made within 50 m of mooring A.

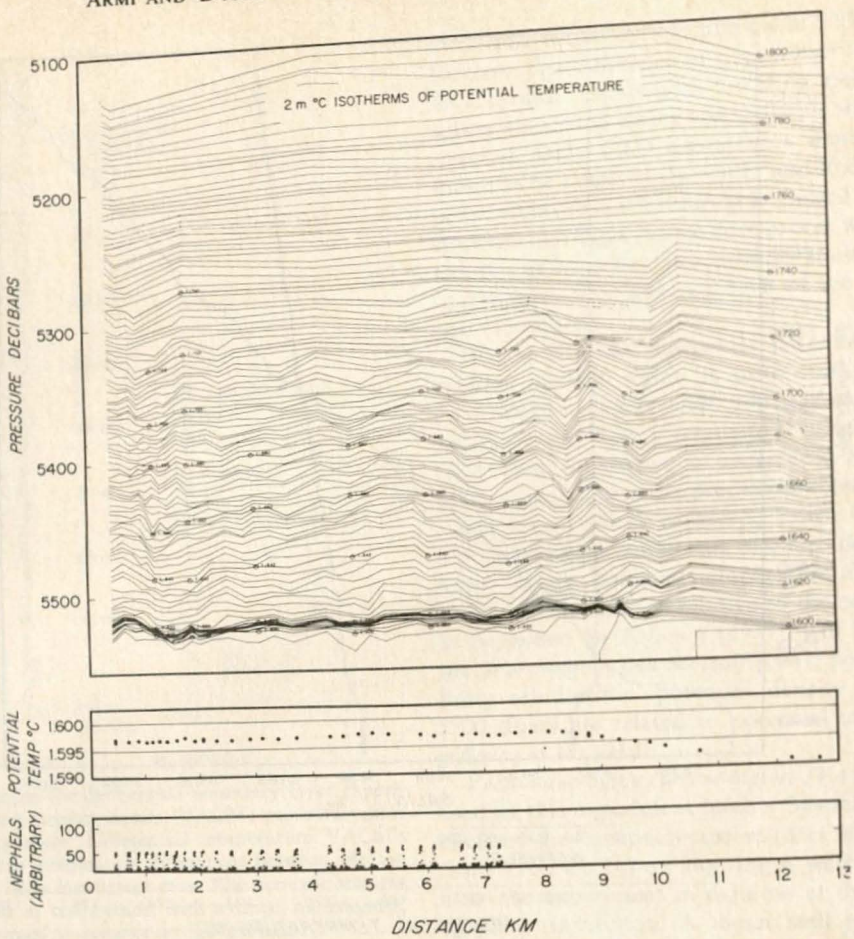

Fig. 5*a*. Section of boundary layer along tow path, 0–13 km, for *Oceanus* 31, station 38. The top panel shows 2-m°C isotherms of potential temperature, created by connecting isotherm crossings on subsequent profiles with straight lines. The middle panel shows mixed layer potential temperature. The bottom panel shows nephels within 100 dbar of the bottom, from 0 to 7.5 km along the tow path. (The nephelometer battery was exhausted beyond 7.5 km.) The bottom distance scale corresponds to the annotation on the tow path shown in Figure 4.

These stations were used to calibrate absolutely the VACM temperatures to the CTD potential temperatures. For the upper instruments the CTD stations were also used in the relative temperature calibration. The final VACM potential temperatures are 1 m°C colder than the CTD potential temperatures for the first CTD survey and 1 m°C warmer for the second and third. Mooring B was calibrated to be consistent with mooring A and nearby CTD measurements. The calibrated potential temperatures from the seven VACM's of mooring A and the two CTD's should be consistent with each other to within 2 m°C.

Nephelometer. This instrument (nephelo is the Greek word for cloud), designed and built at Woods Hole Oceanograhic Institution, was interfaced with the CTD system. White light forward scattering (20°–40°) was measured and recorded along with the other CTD variables. Unlike the CTD, the nephelometer light source was battery powered and limited to ~8 hours of continuous operation. The raw nephelometer signal contains numerous spikes presumably due to the existence of isolated large particles. The largest spikes are often 10 times larger than the standard deviation of the nearby values. Although they are infrequent, these large spikes dominate running averages of the raw data. A 0.33-s average of the raw nephelometer data, excluding large spikes, is called 'nephels' in this paper. The values produced in this way are not sensitive to the exact definition of 'spike' once the biggest spikes have been removed and can be used to distinguish differences between water parcels. The absolute values generated vary between stations because of a small instrumental drift. In relation to the midwater nephels minimum [*Biscaye and Eittreim*, 1977], however, the nephels values are stable. The 3000-dbar nephels value was used as a zero for each station, eliminating the small instrumental drift.

Lagrangian maps. Three CTD surveys near the moored array were made to infer the spatial structure of the boundary layer. However, for many station pairs the spatial separation was of the same order as the displacement of the water by the measured currents during the time between the stations. To simulate a purely spatial survey, each CTD profile was displaced horizontally to the estimated position of the boundary layer at the reference time. This is equivalent to creating a Lagrangian map of the boundary layer from a series of Eulerian measurements at different times. This technique displays the moored time series of potential temperature as a spatial section on the Lagrangian map. Implicit in this scheme is the assumption that the boundary layer does not change significantly over the time of the survey. The survey results are presented on Lagrangian maps, and the validity of this approach is discussed in section 6.

Two of the surveys (*Knorr* 66, stations 7–15, and *Oceanus* 31, stations 2–13) occurred during periods of relatively constant velocity. A single time dependent, uniform velocity field was

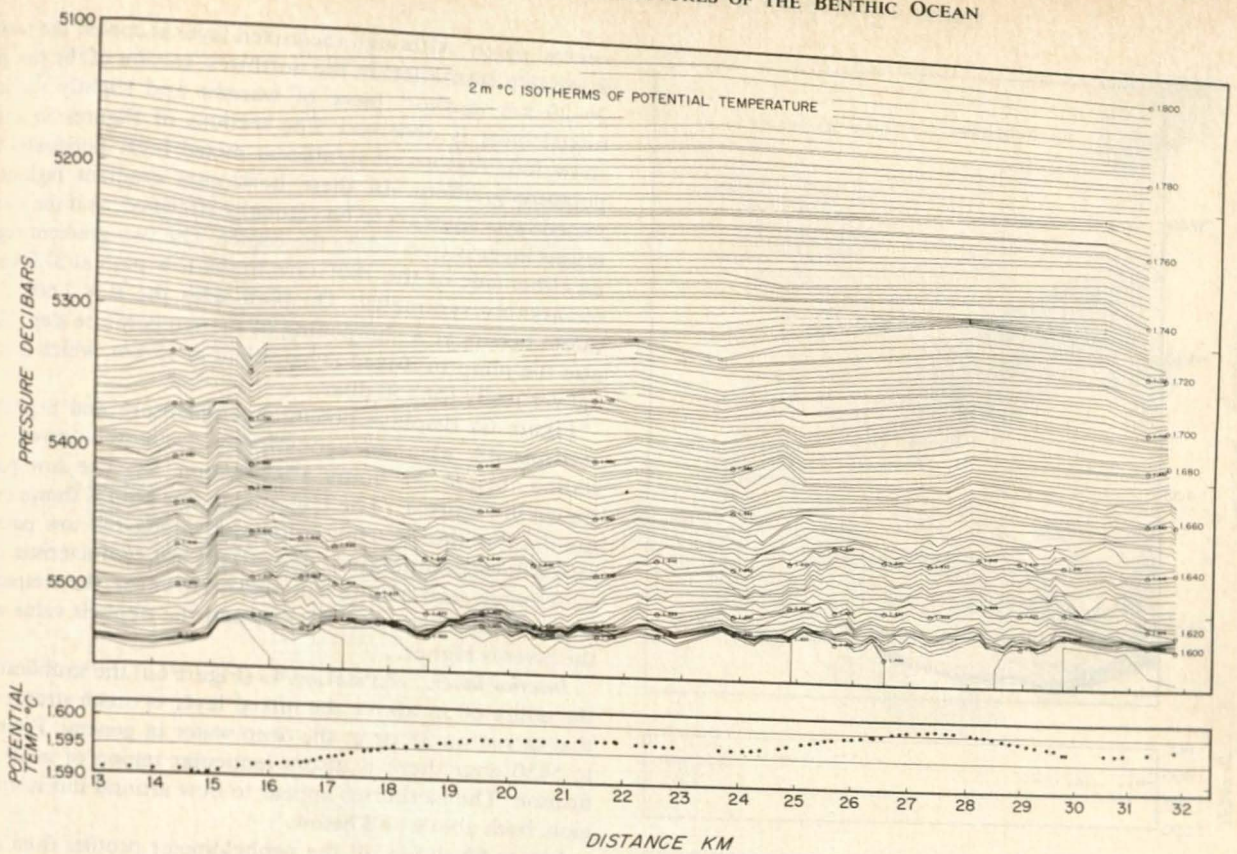

Fig. 5*b*. Continuation of *Oceanus* 31, station 38 section, 13–32 km.

used to create the Lagrangian maps for these surveys. During a third survey (*Oceanus* 31, stations 38–47) the measured acceleration and horizontal shear were significant. A time dependent, inhomogeneous, nondivergent velocity field was used to create the Lagrangian map for this last survey (Figure 7). Since the velocity field was estimated from only two moorings, it contains errors, and the effects of these errors on resultant positions were estimated by varying east/west shears by $\pm 5 \times 10^{-6}$ s^{-1}. The uncertainty in the Lagrangian positions varies for each station, depending primarily on the magnitude of the displacement from its Eulerian position. For the moored data and most of the profiler data the error in relative positions between adjacent stations is less than 2 km. For stations 45 and 46 the error in relative Lagrangian positions may be as large as 5 km. The largest absolute Lagrangian position error is less than 10 km at the extremities of the Lagrangian map.

4. Observations

The structure and velocity field of the benthic ocean over the Hatteras abyssal plain are described below. Detailed spatial observations made primarily with the towed yo-yoing profiler are described first. These data have also been combined with Eulerian observations of velocity and temperature, during the same time period, to create a description in a Lagrangian reference frame. The 3-month-long Eulerian observations are then described. This section is concluded with spatial observations from two additional surveys.

Detailed Spatial Structure

A detailed spatial survey of the boundary layer and the water column immediately above it was made during cruise *Oceanus* 31 on August 14–17, 1977. Bottom mixed layers, interior layers, and bottom temperature patchiness on scales up to ~20 km were observed.

Bottom mixed layers. Figure 3 shows profiles of potential temperature, salinity, and nephels for the first downtrace of station 38. This is a typical boundary layer profile, exhibiting a 24-dbar-thick (~24-m) mixed layer, with constant potential temperature, salinity, and nephels; the layer is capped by a 15-dbar-thick lid through which potential temperature, salinity, and nephels vary rapidly. The mixed layer is colder and more turbid (higher nephels) than the overlying water. Above the mixed layer the nephels gradient is small.

Station 38 was a towed yo-yo station with 145 repeated profiles of the boundary layer along the acoustically navigated tow path shown in Figure 4. (the Lagrangian tow path is shown in Figure 7.) Figures 5*a* and 5*b* display the potential temperature and nephels data along this path. The top panel shows isotherms of potential temperature formed by connecting with straight lines common potential temperatures from individual profiler downtraces. Although the isotherm section extends 500 dbar above the bottom, most of the yo-yos end within 150 dbar of the bottom. The area close to the bottom is more densely sampled, as can be seen in the more detailed structure of the isotherms near the bottom. The very smooth variation of the isotherms in the upper few hundred decibars is due to the small number of mesaurements there. The middle panel shows the bottom potential temperature. The bottom panel shows all nephels values within 100 dbar of the bottom, plotted along the tow path. The upper group of points corresponds to mixed layer nephels, while the separation between the two groups corresponds to the difference in nephels between the interior and the mixed layer.

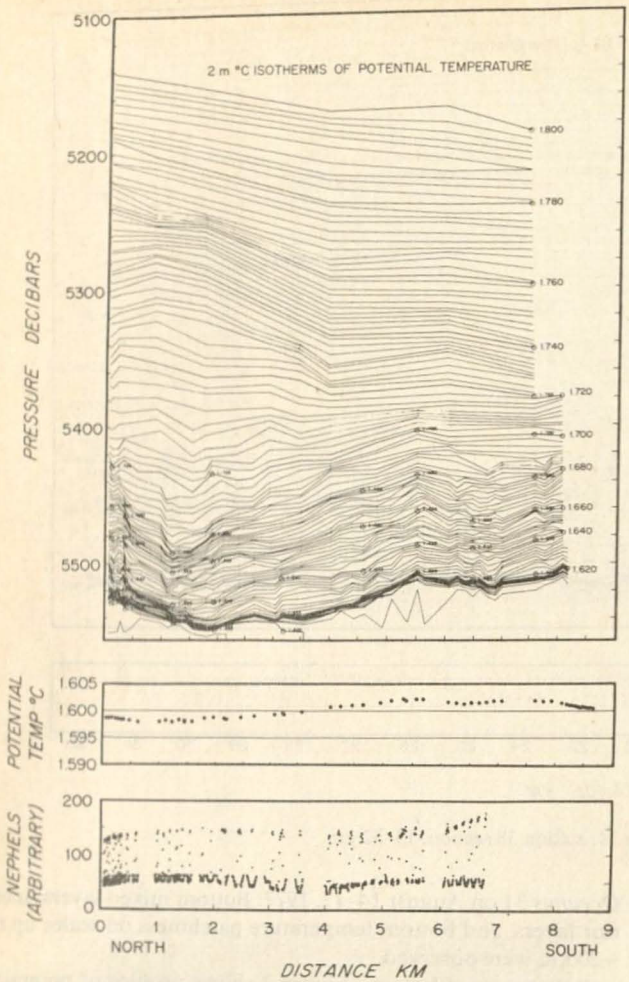

Fig. 6*a*. Section of boundary layer for *Oceanus* 31, station 43. Refer to Figure 5*a* for details. Note the interior lenticular region of weak stratification at the beginning of the section between 5300 and 5450 dbar.

The tow path for station 38 (Figure 4) is roughly a figure eight. If advection by the measured current is removed, the profiles at 5.5 km (1800 August 14, 1977), 21.5 km (0700 August 15, 1977), and 32 km (1548 August 15, 1977) occur within 1 km of the same piece of boundary layer. (Refer ahead to the Lagrangian map (Figure 7).) The density structure is nearly identical at each of these points and for several kilometers around each point, as is illustrated in Figures 5*a* and 5*b*. More than half the length of the section was spent in three visits to this patch of nearly constant mixed layer characteristics. Within the patch the mixed layer potential temperature fluctuates 1 m°C about $\theta = 1.589$°C; the mixed layer height fluctuates 5 dbar about 25 dbar. The mixed layer nephels and the nephels change across the mixed layer top remain constant. The region of large temperature gradient immediately above the mixed layer extends from $\theta = 1.600$°C to $\theta = 1.620$°C throughout the patch; the detailed small-scale structure of this temperature step varies within the patch.

The southeast and northwest sections of the tow path are not in the central patch. The southeast section, extending from 12 to 15 km, is colder and shallower. The mixed layer has a constant potential temperature $\theta = 1.591$°C $\pm$ 1 m°C and a height of 17 $\pm$ 4 dbar. This suggests the existence of another patch of uniform mixed layer to the southeast of the central patch. Although the mixed layer is cooler, the temperature step is smaller. In the northwest section of the tow path, 26–29 km, a short piece of warmer and slightly shallower mixed layer is observed. The sections of Figures 5*a* and 5*b* show four regions of significant mixed layer horizontal temperature gradient. In these horizontal gradient regions the mixed layer appears to be vertically stratified, as if the warmer mixed layer is overriding the cooler. The two gradient regions on either side of the 180° turn in the tow path at 27.5 km are remarkably symmetric. On both sides the $\theta = 1.600$°C isotherm occurs at a sharpening of the temperature step. Notice also the jump in mixed layer height at 15 km, which is coherent vertically for 150 dbar.

Figure 6*a* displays potential temperature and nephels for stations 43, also an acoustically navigated towed yo-yo station, begun 31 hours after station 38. The tow path is shown in Figure 4. (The Lagrangian tow path is shown in Figure 7.) For the first few kilometers along the tow path, the mixed layer temperature and height are characteristic of the main patch seen also in station 38. However, the temperature step is both larger and thicker, and the nephels value within the layer is higher.

Interior layer. At station 43 (Figure 6*a*) the stratification in the entire 60 m above the mixed layer is much stronger than that at station 38 or in the deep water in general. From 5300 to 5450 dbar there is also a lenticular region of weak stratification. The isotherms appear to bow around this interior region, both above and below.

Figure 6*b* shows all the nephelometer profiles from station 43 which extend above 5300 dbar. Three selected isotherms from Figure 6*a* are included to show the boundary of the len-

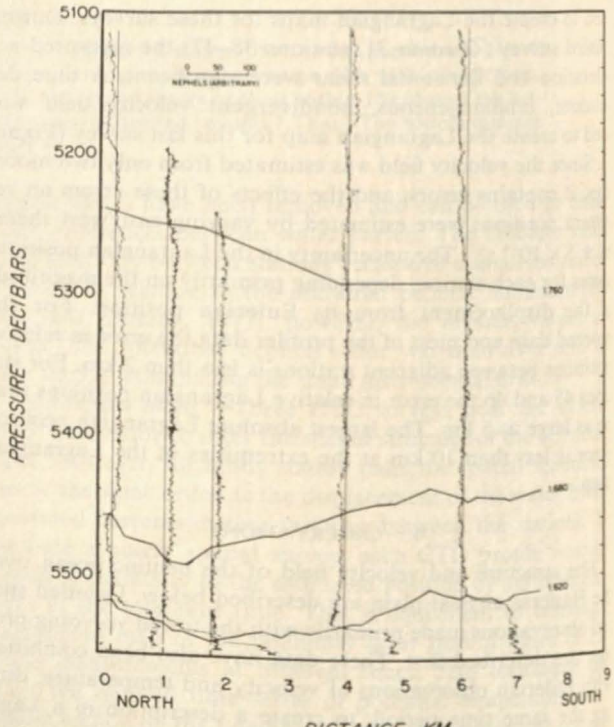

Fig. 6*b*. Nephels profiles from *Oceanus* 31, station 43. Only profiles extending above 5300 dbar are shown. The reference line for each profile corresponds with position along the tow track and with a nephels value of 44. Three potential temperature isotherms from Figure 6*a* are shown to mark the boundary of the interior lenticular region and the top of the mixed layer. Vertical and horizontal scales are the same as those used in Figure 6*a*. Note that the midwater nephels maximum is associated with the interior lenticular region.

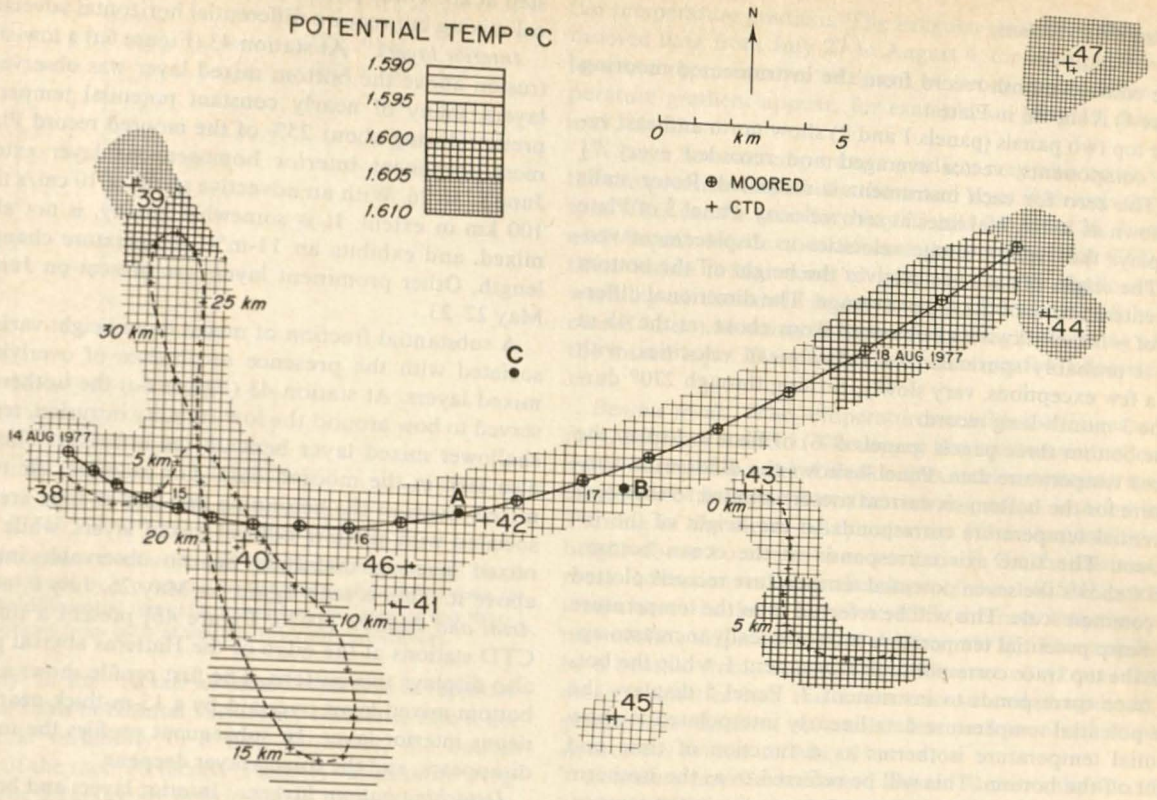

Fig. 7. Lagrangian map of bottom potential temperature using moored and profiler (CTD) data from 0000 August 14 to 1200 August 18, 1977. All Eulerian positions have been translated with the estimated velocity field to positions at 1200 August 16, 1977. Positions of moorings A and B and beacon C are plotted for this reference time. The solid line marks mooring A measurements, annotated at 0000 of each day. Large pluses mark the start of each CTD station; small pluses mark later positions. Dashed lines show Eulerian intervals. These distances correspond to the annotation on the Eulerian tow path (Figure 4). Shading gives mixed layer potential temperature.

ticular region and the top of the mixed layer. As usual, the mixed layer is a nephels maximum. The high-stratification region immediately above the mixed layer is characterized by low nephels, while the lens of weak stratification has higher nephels. The water column is made of several distinct pieces; it could not have been formed by wave straining of a single water type. Since there is a local minimum in nephels immediately above the mixed layer, the lenticular structure could also not have been created by vertical mixing from the bottom but must have involved the horizontal intrusion of water with different nephels. The higher nephels and weak stratification of the lenticular region suggest that it may be a former mixed layer which has detached from the bottom. Further examples of this will be seen below.

The depression of the deeper isotherms around the high-nephels intrusion results in a marked shallowing of the mixed layer at about 2 km along the tow path. This is accompanied by a warming of the mixed layer and an increase in the mixed layer nephels. As occurs in station 38, the mixed layer in the region of horizontal temperature gradient is slightly stratified. At 4 km the deep isotherms begin to rise again, and the mixed layer deepens. The end of the tow seems to show a new patch of mixed layer almost 45 dbar thick with a temperature of around $\theta = 1.602$°C. The low-stability intrusion and the associated nephels maximum have disappeared, but the high-stability region above the mixed layer remains. Note that the interior layer appears to have a strong influence on the bottom mixed layer. Further examples of this will also be seen in the moored data.

Bottom temperature patchiness. Figure 7 combines the 10 CTD stations of this survey and the moored temperature data, discussed next, into a Lagrangian map of bottom temperature. (Lagrangian maps are explained in section 3.) The tow paths of stations 38 and 43, distorted in Lagrangian coordinates, appear as dashed lines. The moored data fall on the solid line, and short CTD stations appear as single points. The main patch of homogeneous mixed layer found at the towed yo-yo station 38, here identified by its potential temperature, is seen to extend 10 km north/south and 20 km east/west. Although it is not shown, the mixed layer height is also constant over this region. South of the main patch the cold shallow patch from station 38 and, further east, the warm deep patch from station 43 are observed. To the east and north of the main patch the mixed layer is warmer.

A horizontal temperature gradient of 4 m°C/km is seen between station 39 and the northernmost point of station 38. The temperature gradient from the four profiles within station 39 is much greater, estimated at 10–20 m°C/km. The largest gradient seen in stations 38 or 43 is only 2–3 m°C/km. The horizontal temperature gradient typical of mesoscale eddies at 4000 m is about 0.3 m°C/km [*Mode Group,* 1978]. Thus the gradient observed at station 39 is 50 times above the mesoscale gradients in this area. Further examples of such temperature gradient regions will be seen in the moored data.

Eulerian Observations

The entire 3-month record from the instrumented mooring (Figure 1) is shown in Plate 1.

The top two panels (panels 1 and 2) show north and east velocity components, vector averaged and recorded every $7\frac{1}{2}$ min. The zero for each instrument is indicated. Rotor stalls are shown as horizontal lines at zero velocity. Panel 3 of Plate 1 displays the 1-day average velocities as displacement vectors. The origin of each vector gives the height off the bottom and centered time of the 1-day average. The directional difference of ~10° clockwise, as observed from above, at the 45-m level is probably spurious. The 1-day mean velocities, with only a few exceptions, vary slowly, turning through 270° during the 3-month-long record.

The bottom three panels (panels 4–6) of Plate 1 display the moored temperature data. Panel 4 shows the differential temperature for the bottom six current meters, plotted so that zero differential temperature corresponds to the height of the instrument. The time axis corresponds to the ocean bottom. Panel 6 shows the seven potential temperature records plotted on a common scale. This will be referred to as the temperature plot. Since potential temperature monotonically increases upward, the top trace corresponds to instrument 1, while the bottom trace corresponds to instrument 7. Panel 5 displays the same potential temperature data linearly interpolated to show potential temperature isotherms as a function of time and height off the bottom. This will be referred to as the isotherm plot. The resolution of temperature is best seen in the temperature plot; however, this plot displays poorly the spatial structure of the temperature field. Structure is best resolved with the isotherm plot. Notice that the height scales on panels 3–5 are identical; they may be overlaid. The bottom time axis is annotated with the times of CTD stations.

Although variations observed at the single mooring contain an unknown combination of temporal and advected spatial variability, the variability observed will be interpreted here as primarily an advected signature of existing horizontal variability. Unlike homogeneous temporal variation, advected variations are not associated with changes in the heat content or potential energy of the fluid. This interpretation will be discussed more fully in section 6.

Bottom mixed layers. These are common in Plate 1. They are seen in the differential temperature plot as a flat trace in the bottom instruments containing no internal wave or advected fine structure signals. Mixed layers are seen in the isotherm plot by the merging of temperature lines from adjacent instruments. The mixed layer heights measured by differential temperature are consistent with those measured by temperature. Because of the finite instrument spacing the mixed layer heights can be resolved only to 10 m, with a minimum measurable height of 15 m. The steplike structure seen in the isotherm plot on May 21 and 22, for example, occurs when the temperature changes significantly in less than 10 m.

Armi and Millard [1976], among others, assumed that the observed boundary layer density structure is formed only by vertically mixing the stratified ocean from below. This hypothesis alone is inadequate to explain the observed density structure. On May 22, for example, a 25-m-high mixed layer is capped by a 80-m°C potential temperature step. This temperature step is equivalent to about 400 m of mixing. On August 3 there is clearly a mixed layer, but there is no temperature step at all. These profiles could not be formed purely by vertical mixing but require differential horizontal advection.

Interior layers. At station 43 (Figure 6*a*) a low-stability intrusion above the bottom mixed layer was observed. Similar layers, many of nearly constant potential temperature, are present during about 25% of the moored record Plate 1. The most prominent interior homogeneous layer extends from June 17 to 26. With an advective speed of 10 cm/s this layer is 100 km in extent. It is somewhat patchy, is not always well mixed, and exhibits an 11-m°C temperature change over its length. Other prominent layers are present on June 5–7 and May 22–23.

A substantial fraction of mixed layer height variation is associated with the presence or absence of overlying interior mixed layers. At station 43 (Figure 6*a*) the isotherms are observed to bow around the low-stability intrusion, resulting in a shallower mixed layer beneath the intrusion. This pattern is also seen in the moored data. For example, the two interior mixed layers at the beginning and end of June are clearly associated with shallow bottom mixed layers, while the deeper mixed layer in mid-June has no observable interior layer above it. This is seen again on May 25, July 6, and July 14. *Armi and Millard* [1976, Figure 4*b*] present a time series of CTD stations at the edge of the Hatteras abyssal plain which also displays this pattern. The first profile shows a 20-m-thick bottom mixed layer overlaid by a 15-m-thick nearly homogeneous interior layer. In subsequent profiles the interior layer disappears, and the mixed layer deepens.

Detaching bottom layers. Interior layers and bottom layers are frequently observed in the moored record to merge with each other (Plate 1). Prominent examples occur on June 28–29 and June 30 to July 2; others are seen on May 24–25, June 1–2, June 26 (2 layers), July 3, and July 23–24.

A most likely source of mixed fluid for an interior layer is a bottom mixed layer. Of 16 interior layers present in the moored record, 6 merge at some point with a bottom layer. This suggests that interior layers are formed by the intrusion of fluid along isopycnals from the bottom mixed layer.

Interior layers may either precede or follow in time their respective bottom mixed layer sources, assuming that advected horizontal variability dominates the Eulerian observations. Both cases are observed with equal frequency.

Bottom mixed layer thickness and temperature. The distribution of mixed layer thickness from the moored record is shown in Figure 8. Mixed layers are most commonly about 20 m thick, while mixed layers 40 m thick or thicker occupy only 11% of the record. The distribution of thickness in each of the three subperiods shown is similar to the distribution for the entire record. The distribution of mixed layer height found by *Millard* [1974] from 44 CTD stations shows heights only 5–10 m thicker.

The moored instruments measure bottom temperature whenever the bottommost instrument is in a mixed layer. Figure 9 shows a histogram of the observed bottom potential temperature; the distribution is quite different in each of the three subperiods. Three months may not be long enough to measure the temperature distribution accurately. Furthermore, during 40% of the record the mixed layer is shallow enough (<20 m) that the bottom temperature cannot be well determined.

The benthic boundary layer was seen in the previously discussed spatial survey to have horizontal variability at scales of

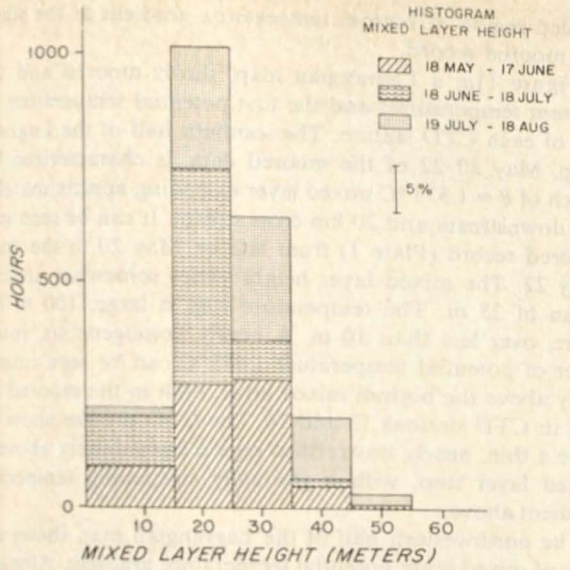

Fig. 8. Histogram of mixed layer heights from mooring A. A mixed layer is defined by a potential temperature change between instruments and a differential temperature within the layer of less than 1 m°C. Contributions from each of three subperiods are shown.

approximately 10 km. At an advected velocity of approximately 10 cm/s this horizontal variability translates into a Eulerian temporal variability of 1 day. However, the bottom temperature of the moored record (Plate 1) varies more irregularly than the Lagrangian map (Figure 7) would indicate. The main $\theta = 1.589$°C patch in Figure 7 is seen from August 14 to 16 in Plate 1. This is a time of exceptionally small potential temperature gradient. The irregular structures seen in the moored data from July 27 to August 4, for example, seem to be more representative. Regions of strong mixed layer temperature gradient appear, for example, on May 19, June 16, and July 23.

A large bottom temperature gradient may also occur when the temperature step above the mixed layer intersects the bottom. This can be seen for May 23 and 24, June 26, June 30, and August 4–6. In the last case there are several CTD stations within 5 km, none of which show any shallowing or warming of the mixed layer (See Fig. 13, which will be discussed later.) Mooring B shows only a slight warming above the mixed layer. This feature is thus only a few kilometers in size.

Benthic front. The temperatures at all levels increase ~50 m°C on June 4 and 5. The upper level instruments then remain warmer for several weeks. This sudden warming is associated with the arrival at the mooring of an interior layer. Turning of the mean 1-day velocities (Plate 1, panel 3) with height above bottom is seen on June 5. On the basis of the mean advection velocity the slope of the 1.625°C potential temperature isotherm is $\sim 4 \times 10^{-2}$ (contrast with the mean thermocline slopes of 2×10^{-3} [*Katz*, 1973]). This appears to be a benthic front. The velocity difference of ~2 cm/s in the mean velocities has the correct sense and magnitude for geostrophic balance. A similar less well resolved frontlike structure is evident on May 24.

Boundary layer turbulence. Figure 10 shows the spectra of horizontal kinetic energy from the VACM instruments. These spectra are similar to those from other measurements in this

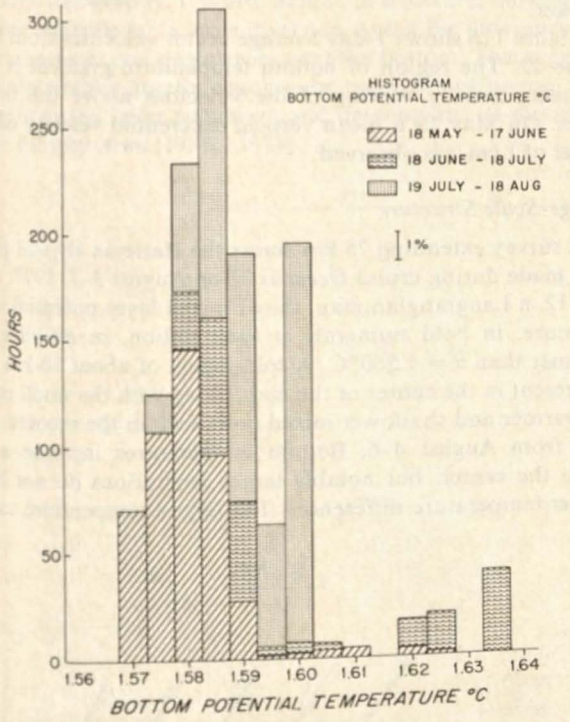

Fig. 9. Histogram of mixed layer potential temperatures from mooring A, defined by the potential temperature at the bottommost instrument whenever the mixed layer is thicker than 20 m. Mixed layer potential temperature, so defined, could not be measured for 40% of the record because mixed layers were smaller than 20 m.

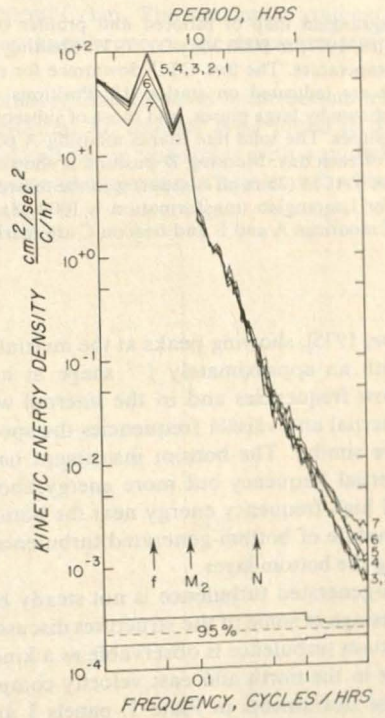

Fig. 10. Horizontal kinetic energy spectra from all seven instruments on mooring A. Labels refer to instrument numbers (refer to Figure 1). Each spectrum is the average of 38 Hanned, overlapped pieces; higher frequencies are band averaged. The 95% confidence limits and the inertial (f), M_2 tidal, and approximate Väisälä (N) frequencies are shown.

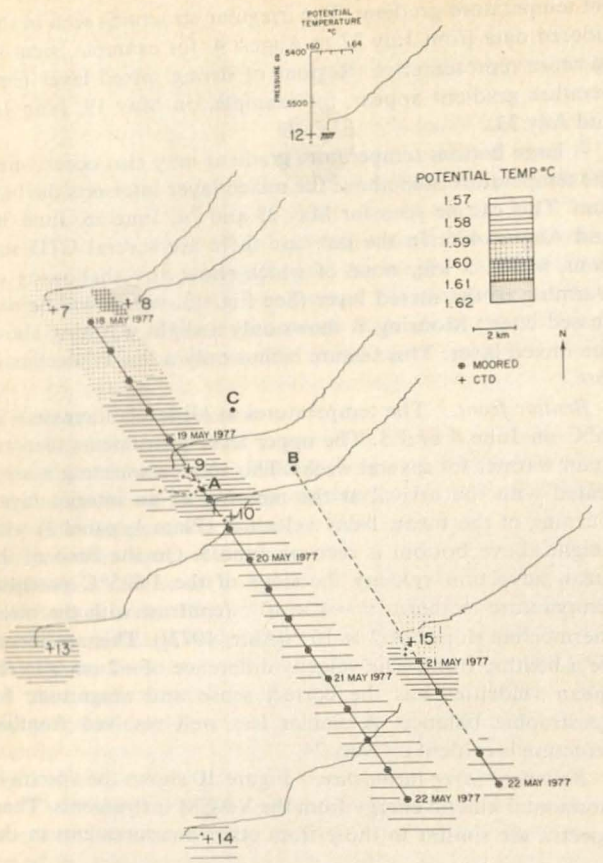

Fig. 11*a*. Lagrangian map of moored and profiler (CTD) data from 0000 May 18, 1977, to 0000 May 22, 1977. Shading shows bottom potential temperature. The first CTD downtrace for each station is shown; scales are indicated on station 12. Positions of the first downtraces are shown by large pluses, and those of subsequent downtraces by small pluses. The solid line marks mooring A positions annotated at 0000 of each day. Mooring B position is shown by a solid line whenever the VACM (35 m off bottom) is in the mixed layer. The reference time for Lagrangian transformation is 1000 May 19, 1977. The positions of moorings A and B and beacon C are marked for this time.

area [cf. *Briscoe*, 1975], showing peaks at the inertial and tidal frequencies with an approximately f^{-2} shape at higher frequencies. At low frequencies and in the internal wave band between the inertial and väisälä frequencies the spectra of all instruments are similar. The bottom instrument has less energy at the inertial frequency but more energy above 1 cph. The additional high-frequency energy near the bottom is presumably a signature of bottom-generated turbulence, responsible for mixing the bottom layer.

This bottom-generated turbulence is not steady but modulated by the passage of some of the structures discussed above. In fact, the bottom turbulence is observable as a kind of high-frequency fuzz in the north and east velocity components of the bottommost instruments in Plate 1, panels 1 and 2. The amplitude of this high-frequency fuzz increases in the deep mixed layers of May 18–20 and July 26–28 and during the passage of the benthic front on June 4–5.

Further Observations of Spatial Structure

A CTD survey was made during cruise *Knorr* 66 on May 17–21, 1977. This survey shows the spatial structure of the extended region of bottom temperature gradient at the start of the moored record.

Figure 11*a*, a Lagrangian map, shows moored and CTD bottom temperatures and the first potential temperature profile of each CTD station. The southern half of the Lagragian map, May 20–22 of the moored data, is characterized by a patch of $\theta = 1.571°C$ mixed layer extending approximately 20 km downstream and 20 km cross stream. It can be seen in the moored record (Plate 1) from late on May 20 to the end of May 22. The mixed layer height varies somewhat around a mean of 25 m. The temperature step is large, 100 m°C or more, over less than 10 m. A nearly homogeneous, interior layer of potential temperature 1.675°C can be seen immediately above the bottom mixed layer, both in the moored data and in CTD stations 13 and 14. The CTD profiles show it to have a thin, nearly unstratified region immediately above the mixed layer step, with a gradually steepening temperature gradient above.

The northwestern half of the Lagrangian map shows a region of mixed layer potential temperature gradient. Along the mean current direction this gradient is about 1.4 m°C/km. However, the bottom temperature map suggests that the bottom isotherms are nearly parallel to the current. A temperature gradient of 8 m°C/km perpendicular to the current occurs near station 8. Station 15 displays a gradient of 8 m°C/km between the first and last cast. It appears therefore that a region of bottom temperature gradient runs diagonally across the map, intersecting mooring A in a region north of May 19. A fairly complex structure is suggested by the moored bottom temperature on May 18 and 19. Southeast of this region is the $\theta = 1.571°C$ patch. Within the gradient region the mixed layer is somewhat thicker, and the temperature step is much thicker.

Figure 11*b* shows 1-day average vector velocities from May 18 to 22. The region of bottom temperature gradient is also characterized by veering of the velocities above the mixed layer. On May 19 a mean vertical differential velocity of the order of 1 cm/s is observed.

Large-Scale Structure

A survey extending 75 km across the Hatteras abyssal plain was made during cruise *Oceanus* 31 on August 3–7, 1977. Figure 12, a Langrangian map, shows mixed layer potential temperature, in bold numerals at each station, in millidegrees warmer than $\theta = 1.580°C$. A cold region of about 10-km size is present in the center of the map, along with the small patch of warmer and shallower mixed layer seen in the moored record from August 4–6. Bottom temperatures increase away from the center, but notably larger separations do not have larger temperature differences. The largest temperature varia-

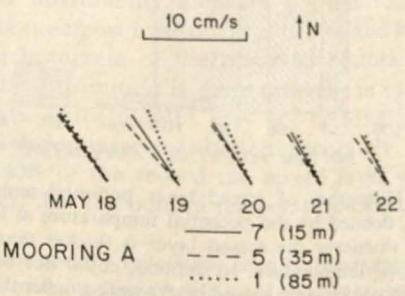

Fig. 11*b*. One day mean vector velocities for instruments 1, 5, and 7 during the interval shown in Figure 11*a*.

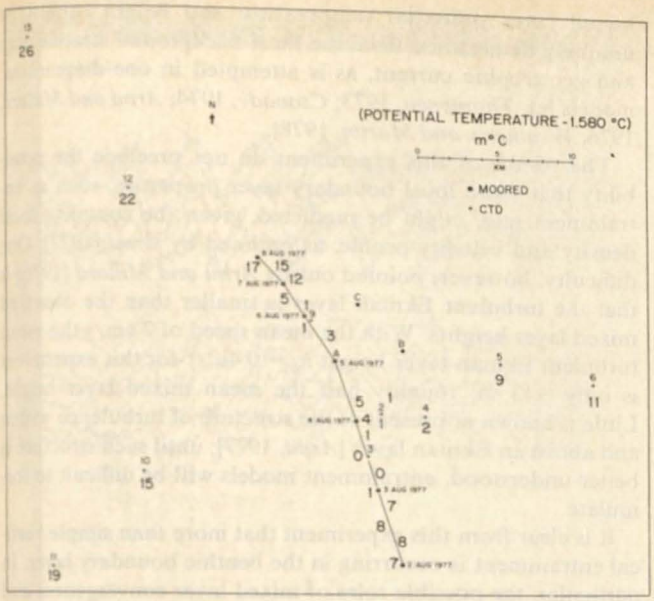

Fig. 12. Lagrangian map for moored and profiler (CTD) data of August 2–8, 1977. The reference time for Lagrangian transformation is 0000 August 5, 1977. Mixed layer potential temperatures above 1.580°C, in millidegrees, are given as bold numerals near the moored and CTD data. The positions of moorings A and B and beacon C are marked at the reference time.

tion occurs on a 10-km scale, in association with the central cold patch. This same scale is evident in the other two bottom temperature maps, Figures 7 and 11*a*.

Figure 13 shows the mixed layer structure found on a 50-km section across the plain. Station 8 is the only station taken in rough topography. It is also unique in structure, showing no bottom mixed layer, a large inversion, and a big difference between uptraces and downtraces near the bottom. This suggests that topography greatly changes the processes of bottom and interior mixed layer formation and detachment, as discussed more fully by *Armi* [1978*a*, 1979].

5. Summary of Observations

The basic three-dimensional scales and structures of the benthic ocean over the Hatteras abyssal plain, as found in moored and profiling measurements, are as follows.

Well-mixed layers extending 5–60 m immediately above the Hatteras abyssal plain are common. Of 29 profiler stations, only one did not have at least a small well-mixed region above the bottom. Over the 3-month moored record the most common mixed layer height was about 20 m. The potential temperature difference between the mixed layer and the overlying stratified water varies from 0 to over 100 m°C. In general, the mixed layers observed could not have been created purely by vertical mixing of a preexisting interior stratification but require, in addition, differential motion between the mixed layers and the overlying water.

Homogeneous or low-stability interior layers above the bottom mixed layer were observed during 25% of the 3-month moored record as well as in the profiler data. These are of the same vertical size as bottom mixed layers and have horizontal extents from 2 to 100 km.

Interior layers and bottom layers are frequently observed in the moored temperature record to merge with each other (cf. June 28–29 and June 30 to July 2 (Plate 1)). Interior layers are probably formed by the intrusion of fluid along isopycnals from a bottom mixed layer.

The presence or absence of interior layers accounts for much of the variation in bottom mixed layer height. Shallower bottom mixed layers are associated with interior layers.

Bottom potential temperature may be constant to within 2 m°C over regions of the order of 10 km or may have gradients of up to 20 m°C/km. The maximum gradients are up to 50 times larger than the mesoscale deepwater temperature gradients.

The nephels (turbidity) level in the bottom mixed layer varies with position. An interior layer found in the profile data (Figures 6*a* and 6*b*) is associated with a midwater maximum in nephels, again suggesting a bottom mixed layer source.

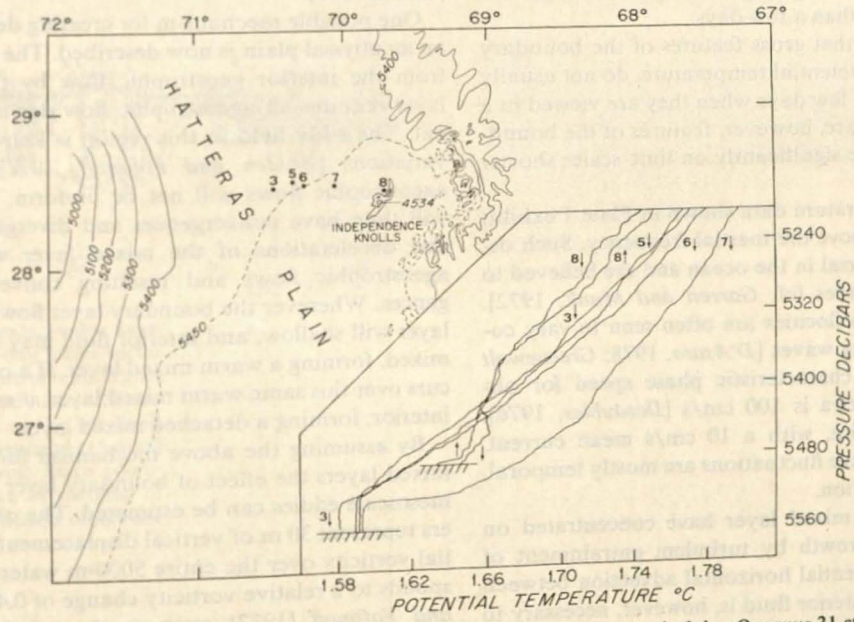

Fig. 13. Large-scale section of the boundary layer across the Hatteras abyssal plain. *Oceanus* 31 station numbers are shown. Note the difference in structure between station 8, taken on the flank of Independence Knolls, and other stations taken on the abyssal plain.

A benthic front with a slope of ~40 m/km is present in the moored data. The velocity difference of ~2 cm/s across the front is of the proper magnitude and direction for geostrophic balance.

Velocity fluctuations above 1 cph increase in energy near the bottom, presumably a signature of turbulence in the mixed layer. These high-frequency velocity fluctuations are modulated by the passage of the structures observed in the moored record.

6. DISCUSSION

Changes in gross features of the bottom boundary layer, such as layer height and potential temperature, have spatial scales of many kilometers. The dominant cause of temporal changes observed at any point, specifically, the main mooring of this experiment, has been interpreted here as being due to advection of this spatial structure. The evidence for this interpretation is as follows.

A single spatial survey presented in Lagrangian coordinates in Figure 7, in section in Figures 5*a* and 5*b*, and in the moored record in Plate 1 from August 14 to 19, 1977, shows approximately the same mixed layer characteristics whenever two observations separated in space and time measure the same piece of mixed layer. The temporal separation of these observations ranges from 7 to 36 hours, the associated Eulerian spatial separations being 3–10 km.

Radon 222 was measured at many of the CTD stations; these measurements have been reported by *Sarmiento* [1978]. Excess radon 222 over the background level originates in the bottom sediments [cf. *Sarmiento et al.*, 1976]; the half-life is 3.8 days. The radon profiles show a nearly constant concentration in the mixed layer; no excess radon is found above the mixed layer. From these profiles, mixing times of less than 3.8 days within the bottom mixed layer and exchange times of greater than 3.8 days with the interior water may be inferred. Unfortunately, no radon measurements were made at times when interior mixed layers were present. The exchange time with the interior inferred from radon profiles supports the interpretation that large-scale Lagrangian temporal changes occur on time scales greater than a few days.

This evidence suggests that gross features of the boundary layer, such as height and potential temperature, do not usually change on time scales of a few days when they are viewed in a Lagrangian frame. There are, however, features of the boundary layer which do change significantly on time scales shorter than a day.

The velocity and temperature data shown in Plate 1 exhibit wavelike oscillations at above the inertial frequency. Such oscillations are nearly universal in the ocean and are believed to be caused by internal waves [cf. *Garrett and Munk*, 1972]. Mixed layer heights and velocities are often seen to vary coherently with the overlying waves [*D'Asaro*, 1978; *Greenewalt and Gordon*, 1978]. The characteristic phase speed for observed internal wave spectra is 100 cm/s [*Desaubies*, 1976]. Therefore at a single point, with a 10 cm/s mean current, these observed internal wave fluctuations are mostly temporal, not advected spatial variation.

Models of the bottom mixed layer have concentrated on predicting mixed layer growth by turbulent entrainment of the overlying fluid. Differential horizontal advection between the mixed layer and the interior fluid is, however, necessary to account for the potential temperature and nephels structures observed in this experiment (cf. Figures 6*a* and 6*b*). Local mixed layer potential temperature and height cannot be uniquely determined from the local background stratification and geostrophic current, as is attempted in one-dimensional models [cf. *Thompson*, 1973; *Csanady*, 1974; *Armi and Millard*, 1976; *Weatherly and Martin*, 1978].

The results of this experiment do not preclude the possibility that some local boundary layer properties, such as entrainment rate, might be predicted, given the complete local density and velocity profile, as outlined by *Armi* [1977]. One difficulty, however, pointed out by *Armi and Millard* [1976] is that the turbulent Ekman layer is smaller than the observed mixed layer heights. With the mean speed of 7 cm/s the mean turbulent Ekman layer height $h_e \sim 0.4u_*/f$ for this experiment is only ~13 m, roughly half the mean mixed layer height. Little is known at present of the structure of turbulence within and above an Ekman layer [*Armi*, 1977]; until such structure is better understood, entrainment models will be difficult to formulate.

It is clear from this experiment that more than simple vertical entrainment is occurring in the benthic boundary layer. In particular, the possible roles of mixed layer convergences and divergences, interior mixed layers, benthic fronts, and differential advection relative to the interior must be considered in any modeling effort.

A dramatic result of this experiment is the frequency with which interior homogeneous layers appear and the suggestion that they result from the detachment of bottom mixed layers (cf. Plate 1). Layering is commonly seen in the upper ocean [*Stommel and Fedorov*, 1967], and the concept of surface boundary layer water penetrating deep into the interior along lines of constant density is at least 40 years old [cf. *Wüst*, 1936, p. 111; *Iselin*, 1939]. *Gregg* [1976] has observed the formation of these layers at the surface and their subsequent movement into the interior. The same phenomenon occurs at the ocean bottom. Since almost all of the deep ocean density surfaces intersect the bottom, detached mixed layers may be present throughout the deep ocean. Other examples from regions of rough and sloping topography have been cited by *Armi* [1978*a*, 1979].

One possible mechanism for creating detached mixed layers on an abyssal plain is now described. The extraction of energy from the interior geostrophic flow by the turbulent mixed layer requires an ageostrophic flow down the pressure gradient. The eddy field in this region is known to have vorticity variations [*Bryden and Fofonoff*, 1977], and hence these ageostrophic flows will not be uniform; the boundary layer will then have convergences and divergences. Accelerations and decelerations of the mixed layer would also produce ageostrophic flows and resulting convergences and divergences. Wherever the boundary layer flow diverges, the mixed layer will shallow, and interior fluid may be drawn down and mixed, forming a warm mixed layer. If a convergence later occurs over this same warm mixed layer, it may be lifted into the interior, forming a detached mixed layer.

By assuming the above mechanism for the detachment of mixed layers the effect of boundary layer convergence on the mesoscale eddies can be estimated. The observed interior layers represent 30 m of vertical displacement. Conserving potential vorticity over the entire 5000-m water column, this corresponds to a relative vorticity change of 0.4×10^{-6} s^{-1}. *Bryden and Fofonoff* [1977] estimate the relative vorticity in the thermocline in this area at 10^{-6} s^{-1} on a 50-km scale. The observed layers therefore represent a substantial conversion of

relative vorticity mediated through the boundary layer. If the boundary layer convergence is primarily due to friction, they also represent a substantial dissipation of the mesoscale eddy vorticity.

Estimates and bounds for the mixing rates both within the mixed layer and between the mixed layer and the interior can be formulated as follows: Geothermal heat flux will heat the mixed layer without changing its salinity. The same potential temperature/salinity relation was, however, always observed, within CTD instrumental error, in the mixed layer and the overlying water. With a relative salinity measurement error of 0.002‰, a geothermal heat flux of 1.3×10^{-6} cal/cm^2/s [*Lee and Uyeda*, 1965], and a 30-m mixed layer an exchange time between the mixed layer and the interior of less than 600 days is required (see also *Armi* [1977]). The above upper bound complements the lower bounds provided by the radon 222 measurements of *Sarmiento* [1978] already discussed. Combined, these measurements suggest mixing times of less than 3.8 days within the mixed layers and an exchange time of between 3.8 and 600 days with the interior.

Since interior mixed layers were observed during 25% of the moored record and not the entire record, they presumably are dissipated, either by vertical mixing or by horizontal shearing and interleaving, as cartooned by *Armi* [1978*a*]. The time scale for these processes must be similar to that of the formation, roughly 100 days, since the interior layers fill only a fraction (~25%) of the fluid immediately above the bottom mixed layer. Transit times, from the mooring site to topography at the edge of the abyssal plain or another bottom contact again on the abyssal plain itself, of 100 days are possible with the mean speed of 7 cm/s observed during this experiment.

This paper has emphasized aspects of the benthic ocean as revealed primarily by mean current, temperature, salinity, and nephelometer data. A detailed analysis of the velocity data will be presented in a later paper.

Acknowledgments. We are particularly grateful to the WHOI buoy group for careful preparation of the current meters and moorings used in this experiment and subsequent data processing. We thank J. Dean for the attention that he paid to the differential temperature measuring current meters, D. Koehler for design and construction of the nephelometer, and the WHOI CTD group. We thank one of the reviewers for pointing out the frequency of merging between the bottom and interior mixed layers. This research was supported by the Office of Naval Research under contract N00014-76-C-0197, NR 083-400 and by the National Science Foundation under grant OCE 76-81190. Partial support for one of us (E. D'Asaro) was provided by a National Science Foundation graduate fellowship. This is contribution 4359 from the Woods Hole Oceanographic Institution.

REFERENCES

Armi, L., The dynamics of the bottom boundary layer of the deep ocean, in *Bottom Turbulence, Proceedings of the 8th International Liège Colloquium on Ocean Hydrodynamics*, edited by J. C. J. Nihoul, pp. 153–164, Elsevier, New York, 1977.

Armi, L., Some evidence for boundary mixing in the deep ocean, *J. Geophys. Res., 83*, 1971–1979, 1978*a*.

Armi, L., Mixing in the deep ocean—The importance of boundaries, *Oceanus, 21*(1), 14–19, 1978*b*.

Armi, L., Reply, *J. Geophys. Res., 84*, 5097–5098, 1979.

Armi, L., and R. C. Millard, The bottom boundary layer of the deep ocean, *J. Geophys. Res., 81*(27), 4983–4990, 1976.

Biscaye, P. E., and S. L. Eittreim, Suspended particulate loads and transports in the nepheloid layer of the abyssal Atlantic Ocean, *Mar. Geol., 23*, 155–172, 1977.

Briscoe, M. G., Preliminary results from the trimoored Internal Wave Experiment (Iwex), *J. Geophys. Res., 80*(27), 3872–3884, 1975.

Bryden, H. L., Horizontal advection of temperature for low frequency motions, *Deep Sea Res., 23*(12), 1165–1174, 1976.

Bryden, H. L., and N. P. Fofonoff, Horizontal divergence and vorticity estimates from velocity and temperature measurements in the Mode region, *J. Phys. Oceanogr., 7*(3), 329–337, 1977.

Bush, P. A., Bathymetry of the Mode-1 region, *Deep Sea Res., 23*(12), 1105–1113, 1976.

Csanady, G. E., Equilibrium theory of the planetary boundary layer with an inversion lid, *Boundary Layer Meteorol., 6*, 63–79, 1974.

D'Asaro, E., Mixed layer velocities induced by internal waves, *J. Geophys. Res., 83*, 2437–2438, 1978.

Dean, J. P., A moored instrument for vertical temperature gradients, *J. Geophys. Res., 84*, 5089–5091, 1979.

Desaubies, Y. J. F., Analytical representation of internal wave spectra, *J. Phys. Oceanogr., 6*, 976–981, 1976.

Eittreim, S., P. E. Biscaye, and A. F. Amos, Benthic nepheloid layers and the Ekman thermal pump, *J. Geophys. Res., 80*(36), 5061–5067, 1975.

Fofonoff, N. P., Computation of potential temperature for seawater from arbitrary reference pressure, *Deep Sea Res., 24*, 489–491, 1977.

Fofonoff, N. P., S. P. Hayes, and R. C. Millard, Jr., W.H.O.I./Brown CTD microprofiler: Methods of calibration and data handling, *Ref. 74–89*, Woods Hole Oceanogr. Inst., Woods Hole, Mass., 1974.

Garrett, C., and W. Munk, Space-time scales of internal waves, *Geophys. Fluid Dyn., 2*, 225–264, 1972.

Greenewalt, D., and C. M. Gordon, Short-term variability in the bottom boundary layer of the deep ocean, *J. Geophys. Res., 83*, 4713–4716, 1978.

Gregg, M. C., Finestructure and microstructure observations during the passage of a mild storm, *J. Phys. Oceanogr., 6*, 528–555, 1976.

Iselin, C. O., The influence of vertical and lateral turbulence on the characteristics of waters at middepths, *Eos Trans. AGU*, 414–417, 1939.

Katz, E., Profile of an isopycnal surface in the main thermocline of the Sargasso Sea, *J. Phys. Oceanogr., 3*(4), 448–457, 1973.

Lee, W. H., and S. Uyeda, Review of heat flow data, in *Terrestrial Heat Flow, Geophys. Monogr. Ser.*, vol. 8, pp. 87–190, AGU, Washington, D. C., 1965.

McCullough, J., Vector averaging current meter speed calibration and recording technique, *Ref. 75–44*, Woods Hole Oceanogr. Inst., Woods Hole, Mass., 1975.

Millard, R. C., Bottom layer observations from Mode and Iwex, *Mode Hot Line News 60*, Woods Hole Oceanogr. Inst., Woods Hole, Mass., 1974.

Mode-1 Atlas Group, *Atlas of the Mid-Ocean Dynamics Experiment (Mode-1)*, MIT Press, Cambridge, Mass., 1977.

Mode Group, The Mid-Ocean Dynamics Experiment, *Deep Sea Res., 25*(10), 859–910, 1978.

Pak, H., and J. R. Zaneveld, Bottom nepheloid layers and bottom mixed layers observed on the continental shelf off Oregon, *J. Geophys. Res., 82*, 3921–3931, 1977.

Payne, R. E., A. L. Bradshaw, J. P. Dean, and K. E. Schleicher, Accuracy of temperature measurements with the VACM, *Ref. 76–94*, Woods Hole Oceanogr. Inst., Woods Hole, Mass., 1976.

Phillips, J. D., A. H. Driscoll, K. R. Peal, W. M. Marquet, and D. M. Owen, A new undersea geological survey tool: Angus, *Deep Sea Res., 26*, 211–225, 1979.

Sarmiento, J. L., A study of mixing in the deep sea based on STD, radon-222 and radium-228 measurements, Ph.D. thesis, Columbia Univ., New York, 1978.

Sarmiento, J. L., H. W. Feely, W. S. Moore, A. E. Bainbridge, and W. S. Broecker, The relationship between vertical eddy diffusion and buoyancy gradient in the deep sea, *Earth Planet. Sci. Lett., 32*, 357–370, 1976.

Stommel, H., and K. N. Fedorov, Small-scale structure in temperature and salinity near Timor and Mindanao, *Tellus, 19*, 306–325, 1967.

Thompson, R. O., Stratified Ekman boundary layer models, *Geophys. Fluid Dyn., 5*, 201–210, 1973.

Thorndike, E. M., A deep-sea photographic nephelometer, *Ocean Eng., 3*, 1–15, 1975.

Weatherly, G. L., and P. J. Martin, On the structure and dynamics of the oceanic bottom boundary layer, *J. Phys. Oceanogr., 8*(4), 557–570, 1978.

Weatherly, G. L., and P. P. Niiler, Bottom homogeneous layers in the Florida current, *Geophys. Res. Lett., 1*(7), 316–319, 1974.

Wimbush, M., and W. Munk, The benthic boundary layer in *The Sea*, vol. 4, part 1, John Wiley, New York, pp. 731–758, 1970.

Worthington, L. V., and W. G. Metcalf, The relationship between potential temperature and salinity in deep Atlantic water, *Rapp. Process. Verb. Reunions Cons. Perma. Int. Explor. Mer, 149,* 122–128, 1961.

Wüst, G., Die Stratosphäre des Atlantischen Ocean, *Wiss. Ergeb. Deut. Atlantischen Exped. Vermess. Forschungsschiff Meteor 1925-1927, II*(I), 1936.

(Received July 17, 1979;
revised September 14, 1979;
accepted September 17, 1979.)

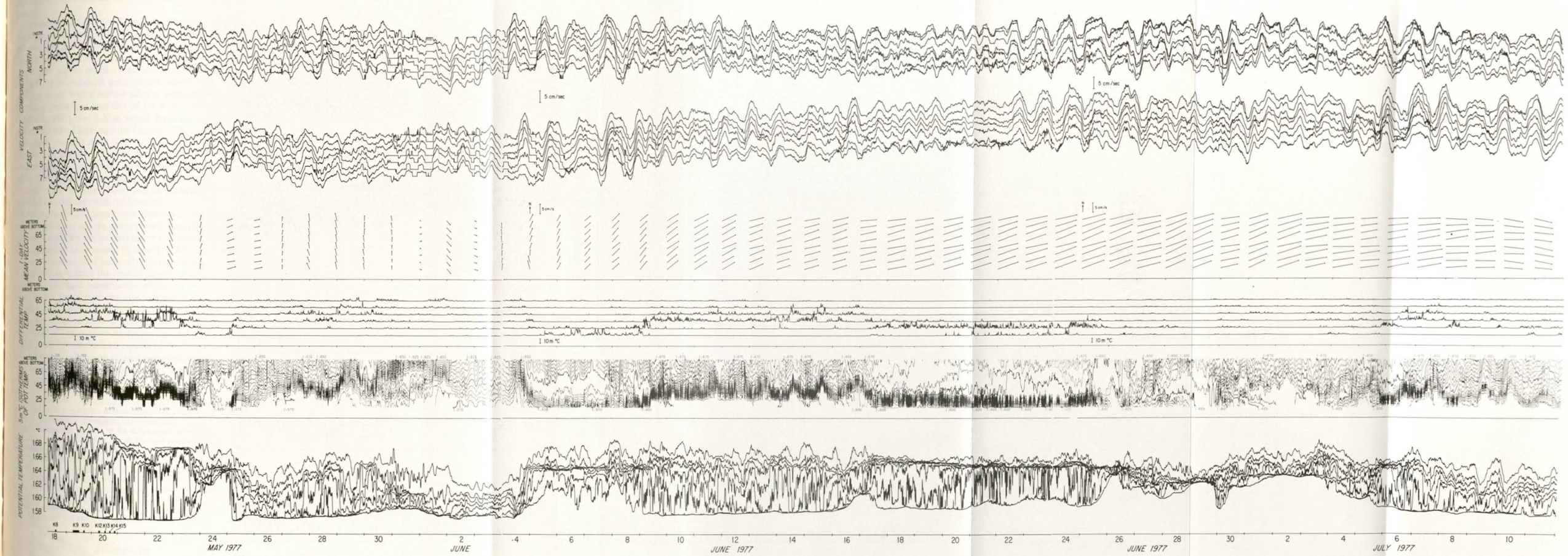

Plate 1. Velocity and potential temperature data from mooring A (refer to Figure 1). Panels 1 and 2 (top two panels): north and east velocity components, vector averaged and recorded every 7½ min. The zero for each instrument is offset as indicated. Rotor stalls are shown as horizontal lines at zero velocity. Panel 3: 1-day mean vector velocities from each instrument plotted daily. The origin of the vector gives central time and height off bottom. Data at 75 m are interpolated from adjacent instruments. Panel 4: Differential temperature (difference in temperature between the top and the bottom of the 1.74-m instrument case) for instruments 2–7. Flat traces correspond to no differential temperature (i.e., the instrument is in a mixed layer). The plot for each instrument is offset vertically, corresponding to its height off bottom as indicated on the left-hand scale. Panel 5: 5-m°C time/height isotherms of potential temperature linearly interpolated for each data cycle. No isotherms are plotted below the bottom instrument (15 m off bottom). The peculiar step structure on May 22, for example, results from linear interpolation. Panel 6: Potential temperature/time plots for all seven instruments. Since potential temperature increases upward, the top trace corresponds to the top instrument, and the bottom trace to the bottom instrument. Mixed layers are shown by merging of adjacent potential temperature lines. Station Annotation: Times and durations of CTD stations are shown above the bottom time axis. K indicates *Knorr* 66 stations; others are *Oceanus* 31 stations. Eulerian positions are shown in Figure 2, and Lagrangian positions in Figures 7, 11*a*, and 12.

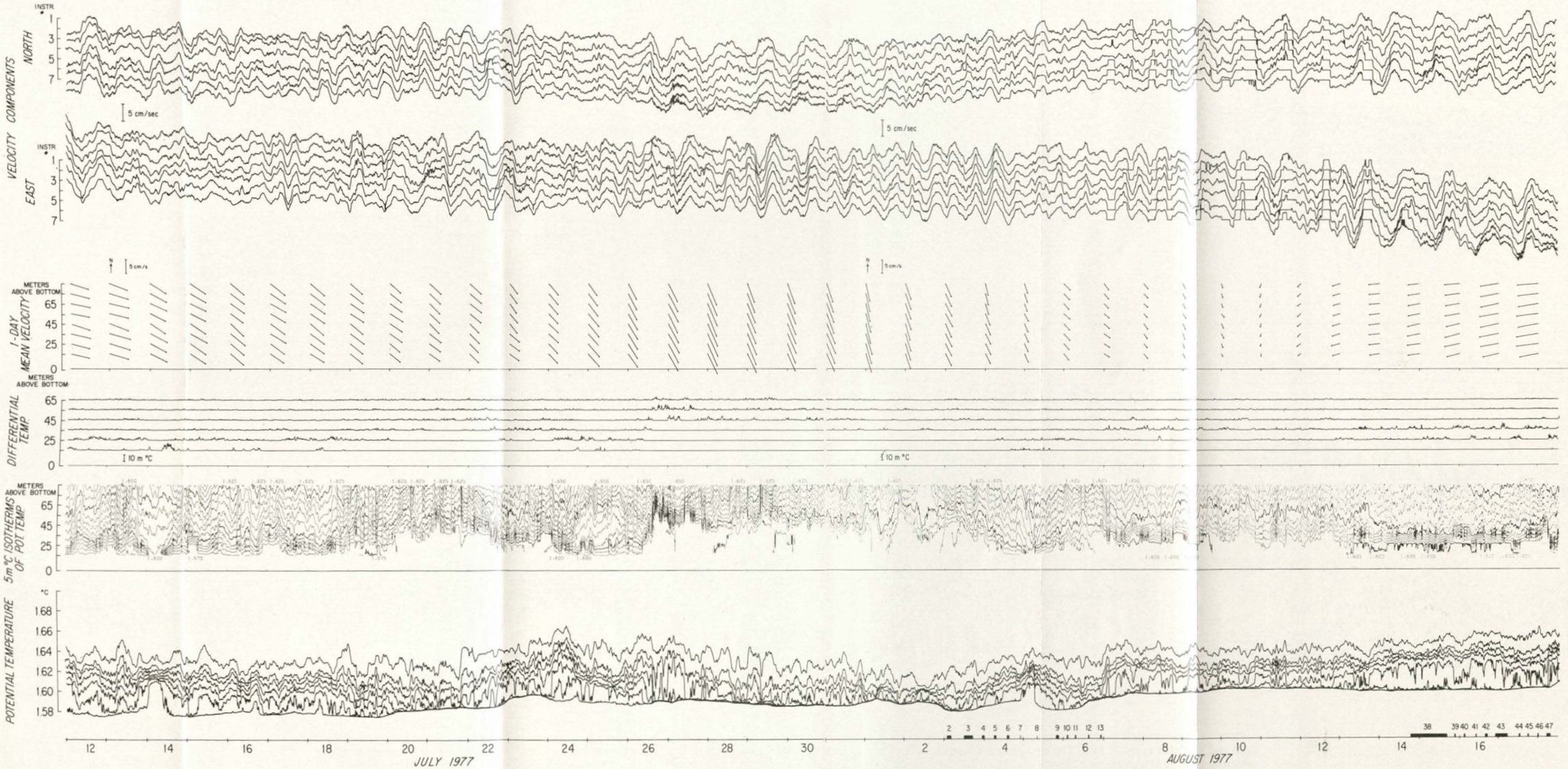

Plate 1. (continued)